Passive reception of Two-Way Satellite Time and Frequency Transfer (TWSTFT) signals from a geostationary satellite, or GPS upside down

J.-M Friedt JMFRIEDT@FEMTO-ST.FR
FEMTO-ST time & frequency department, Besançon

Abstract

We explore the reception of signals emitted by European time and frequency metrology Observatories and broadcast by a geostationary satellite by processing signals recorded from a consumer television reception parabola using a software defined radio.

Temps atomique international (TAI, atomic international time) is defined by comparing multiple clocks distributed on various continents. With its snail pace of 300 m per microsecond, light (or any other electromagnetic wave) is a poor communication medium for sharing timing signals with sub-nanosecond accuracy as requested by some of current technological applications on ranges as large as a few kilometers to thousands of kilometers. Every day, national metrology institutes share information allowing for compensating the time of flight of the electromagnetic wave emitted from ground to a geostationary satellite broadcasting the signal back to ground and observe the drift of their respective clocks. Can we benefit from these links to synchronize our own clocks, and achieve such a result at a reasonable financial cost? We will show how to divert a consumer grade television reception parabola dish from its original purpose, fitted with a software defined radio (SDR), to receive and decode this signal.

1. Introduction

Time and frequency are two closely linked quantities: frequency (expressed in hertz) is the inverse of time (expressed in second). This formal definition, as found in a dictionary, does not bring any insight into the technical challenges for sharing time over the triviality of the concept of frequency. A core difference between these two quantities is bandwidth needed to share frequency or time: while a frequency is characterized by a continuous sine wave as reproducible as possible from one period to the next – hence represented by a Dirac function after computing the Fourier transform to reach the spectral domain – time requires differentiating the evolution of the signal, and we will see how this operation is intrinsically broadband requiring wide spectral components. Technologically, the two operations are orthogonal and the requirements for transmitting these two information are very different (Fig. 1).

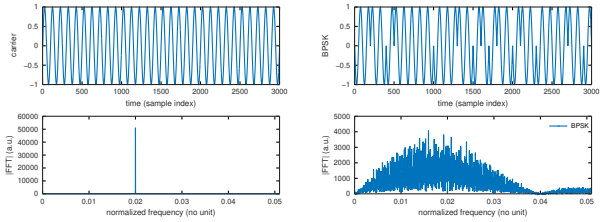

Figure 1. Left: a continuous wave (CW) only carries a frequency information but no timing information, all periods looking alike. Right: in order to differentiate successive periods, a phase rotation, here 0 or π for a Binary Phase Shift Keying (BPSK) modulation, is applied to the CW carrier. The length of the sequence that never repeats leads to the uncertainty on time transfer when correlating the received signal with the randomly *but known* varying phase pattern applied to the carrier. Top the time-domain evolution of the signal and bottom its spectrum, emphasizing that timing resolution is inversely proportional to the bandwidth occupied by the signal.

Formally, a frequency f is the linear derivate of the phase Φ when expressing a periodic signal v as a function of time t such as $v(t) = \sin(\Phi)$ where $\Phi = 2\pi ft + \varphi(t)$, $\varphi(t)$ the random phase fluctuations. The signal v is narrowband, with a spectral component mainly at f but spread around the carrier due to φ. Frequency metrology aim at knowing as accurately as possible f with as little variations as possible from one measurement to the next, while the users of radiofrequency signals (e.g. digital communications or RADAR measurements) aim at keeping f as stable as possible during the time of flight of the wave between speakers or the emitter, the target and the receiver so that any variation of the received signal frequency can be unambiguously attributed to the carried information – phase modulation or velocity of the target inducing a Doppler shift – and not

Proceedings of the 1st GNU Radio Conference, Copyright 2016 by the author(s).

to the local oscillator. Frequency is hence an information with little interest since it does not evolve and we only try to reproduce as closely as possible the same process from one period to the others, for example by using an as high quality factor resonator as possible storing as much energy as possible to make it insensitive to external disturbances (Fig. 1, gauche).

Time is much more interesting since it is intrinsically a broadband information, with a broad spectral occupation, or in other terms the timing resolution dt is inversely proportional to occupied bandwidth B: for a RADAR application, the range resolution is $c/(2B)$ since the the resolution on the two-way time of flight (hence the 1/2 factor) is inversely proportional to the inverse of the bandwidth, time being converted to distance by multiplying with the speed of light $c = 300$ m/μs. All periods of a periodic signal look alike and do not carry any timing information: we must find a trick to encode time on the carrier in order to differentiate the various periods. This problem is the core issue of GPS but all radiofrequency links sharing time in general (Fig. 1, right) as will be described in section 2.

Atomic clocks currently used to define international atomic time exhibit a stability of a few picoseconds per second (10^{-12} relative stability (1)) that a naive transfer approach might consider requiring a few GHz bandwidth – inverse of the targeted timing resolution – for comparisons. Worse, the time of flight between ground, a geostationary satellite – selected so that the parabola such as the one used for receiving television targets a fixed location, and most significantly to avoid Doppler shift induced by the motion of the satellite – at an altitude of 36000 km, and the ground, induces a delay of 240 ms at least. How then can a "reasonable" bandwidth (less than a television channel using 30 to 50 MHz according to ETSI EN 300 421) allow for sharing timing information between metrology laboratories meeting these requirements? Understanding these mechanisms might allow us to benefit from these signals for our own use, understanding their limitations and the challenges. But most interestingly, by understanding the solutions to the these challenges, we will use the signals transmitted every day and broadcast over the European and North-American continents for our own purposes, for example for comparing and controlling the frequency of local oscillators, and maybe even tune the receiver local clock time.

Geostationary satellites as radiofrequency link relays
The use of geostationary satellites for long range communication is driven, as was identified by A.C. Clarke in 1945 (7), by the curvature of the Earth that leads to locating the relay as far away from the surface of the Earth as possible to cover an area as wide as possible. Trigonometric considerations tell us that an emitter located at an altitude h over the surface of the Earth with radius R_t allows for communicating at a range of $R\vartheta$ with $cos\vartheta = \frac{R_t}{R_t+h}$: for example for the International Space Station orbiting at an altitude of $h = 400$ km, $\vartheta = 2200$ km against 9100 km for a geostationary satellite at $h = 36000$ km. This altitude is selected so that the satellite orbital period is the same than the Earth rotation and hence the satellite appears at a fixed location in the sky over time, easing the reception with a high gain and hence strongly directional antenna without need for tracking a target appearing moving in space.

While this work is closely linked to the professional activity of its author, it diverges with the aim of sharing the information with an audience unable to emit but only allowed to listen, but most significantly we have made sure that all information shared in this document can be found freely in the publicly available literature as referenced in the bibliography link associated with each statement. Obviously, knowing the answer makes the search on the web much easier !

2. Principles of time transfer

Converting a periodic signal – an electromagnetic wave for example – to a time transfer medium, we must **spread the spectrum**. A periodic signal is characterized by three (actually two) quantities: its amplitude, its frequency and its phase (the frequency being only the linear drift over time of the phase). For differentiating the successive periods by imprinting a timing information, we can tune each one of the quantities, amplitude or phase. Optical links must work with amplitude only, but when using radiofrequency signals we can manipulate the phase, leading to a much more efficient use of the spectrum. In the case of GPS, the phase jumps between 0 and π to imprint a binary information allowing for encoding time. The period with which the code repeats – the length of the code in a digital approach – defines the uncertainty on the time of flight, also known as the Pulse Repetition Interval in RADAR systems: a short code induces a strong uncertainty on the time of flight, a long code reduces the uncertainty but requires larger computational capability for identifying the code in the noisy received signal. The rate at which the code is transmitted determines the resolution with which the time of flight will be measured. The transmitted signal might be a sine wave, but could be any electromagnetic signal and even noise, as long as *the emitter has taken care of recording the transmit-*

ted pattern in order to identify the delayed repetition of this pattern and determine the time of flight as was discussed in the noise RADAR implementation (2).

Indeed, how can we determine the time of flight between emission and reception? The problem lies in finding a pattern $p(t)$ – random but *known* (3) – emitted at a given time, in the noisy signal $s(t)$ received: the optimal matched filter is the correlation of s with p expressed as

$$xcorr(p,s)(\tau) = \int s(t)p^*(t+\tau)dt$$

with * the complex conjugate when handling complex quantities as usually done in software defined radio at the output of an IQ detector, or in other words computing the product of the pattern with the signal time shifted by τ and assessing for each τ the mean power resulting from the integration. If s and p exhibit a null mean value, then their integral is 0 except if for a given time delay τ, p is found in s: in this case, the positive parts of the signal match the positive parts of the pattern to lead to a positive product, and so do the negative parts of the signal matching the negative parts of the pattern also leading to a positive product, and the integral accumulates energy in a sharp correlation peak, whose width is inverse of the transmitted signal bandwidth. This principle of spectrum spreading by phase modulation of the carrier is used by all instruments designed for time transfer, including global navigation satellite system constellations, and time and frequency transfer using a geostationary satellite does not break the rule.

Hence, the program of the investigation is found:

1. learn how to receive the microwave signals transmitted from ground by metrology instruments and broadcast over Europe and the North-American continents (Fig. 2) by the relay geostationary satellite,
2. identify the encoding and the patterns $p(t)$ imprinted on the carrier phase to transmit timing information,
3. decode these signal and compare with the local clock – the one we wish to calibrate also used for clocking the software defined radio receiver (4; 5; 6) used for receiving the signals
4. identify the limitation of the one-way communication link, most significantly because a geostationary satellite we might believe to be at a fixed location in the sky actually swings around its equilibrium point depending on the forces generated by the Moon, Sun and planets.

We will no consider here how to control the local clock, but how the television reception parabola dish allows for measuring the motion of the satellite at a distance of more than 36000 km from the receiver, and how these results are in excellent agreement with the measurements shared by the *Bureau International des Poids et Mesures* (BIPM – International Agency for Weights and Measurements) which centralizes the information collected every day.

3. Practical aspects of time transfer

The first web site that will provide the most relevant information is the file server of BIPM at https://webtai.bipm.org/ftp/pub/tai/data/2022/time_transfer/twstft/ which groups all the information shared between primary time and frequency metrology laboratories. The files in these folders, classified depending on their origin, include in their header the carrier frequency and the coordinates of the parabola broadcasting towards the geostationary satellite.

For example https://webtai.bipm.org/ftp/pub/tai/data/2022/time_transfer/twstft/roa/twroa59.729 starts with

```
...
* LAB       ROA
* ES ROA01  LA: N 36 27 51.530       LO: W 006 12 22.333   HT: +0074.67 m
...
* LINK   23 SAT: TELSTAR 11N         NLO: E 322 27 00.000  XPNDR: 999999999 ns
*           SAT-NTX: 10953.9500 MHz  SAT-NRX: 14253.9500 MHz  BW:   4.1 MHz
```

telling us that the Spanish Navy Observatory (https://en.wikipedia.org/wiki/ROA_Time) is located in Cádiz at a latitude of 36 degrees North and 6 degrees longitude West and uplinks around 14 GHz while the downlink frequency is 10.95395 GHz (8) with a communication bandwidth of about 4.1 MHz. We hence know which satellite to aim the parabola for (Telstar-11N(9)) and which frequency to listen to, sampling with a bandwidth easily reached by most software defined radio receivers. Aiming the parabola towards the satellite is achieved by following the information provided by https://www.dishpointer.com/: from Besançon in Eastern France, Telstar-11N located at 37.5 degrees West over the Atlantic is located at an elevation of 21.4° and 229.7° azimuth with respect to the magnetic North. Considering the small 60-cm diameter receiving parabola, the decimal value does not matter much, the antenna aperture being broad enough to easily aim towards the satellite. Notice though that the geostationary orbit is so crowded that erroneously aiming at the neighboring satellite is easy (Fig. 3) ! We have indeed spent a few weeks trying to detect the targeted signal from the satellite neighbor to Telstar-11N, due to the coarse manual aiming despite the availability of a broadband spectrum analyzer allowing for easily collecting the powerful emissions of each satellite along the equator. Fig. 3 illustrates how crowded the orbit is with one satellite located about every 0.3° along the longitude, requiring

Figure 2. Map of the European and North-American Observatories in charge of sharing time and frequency, complemented with the location of Besançon (France) where the measurements are performed (LTFB) as well as the location over the Atlantic Ocean of the geostationary Telstar-11N satellite.

https://www.n2yo.com/satellites/?c=10&srt=11&dir=1 dishpointer.com

INTELSAT 14	36097	2009-064A	November 23, 2009	1436.1	45° W
USA 7	15453	1984-129A	December 22, 1984	1456.6	44.4° W
INTELSAT 32E (SKY BRASIL 1)	41945	2017-007B	February 14, 2017	1436.1	43.2° W
INTELSAT 11 (PAS 11)	32253	2007-044B	October 5, 2007	1436.1	42.9° W
SESAT 2 (EXPRESS AM-22)	28134	2003-060A	December 28, 2003	1449.3	42.9° W
USA 170	27875	2003-040A	August 29, 2003	1436.1	42.3° W
EUTELSAT 2-F2	21056	1991-003B	January 15, 1991	1455.4	42.2° W
KALPANA 1 (METSAT 1)	27525	2002-043A	September 12, 2002	1464.3	42.1° W
EXPRESS AM-11	28234	2004-015A	April 26, 2004	1451.1	41.5° W
TDRS-12	39504	2014-004A	January 23, 2014	1436	40.9° W
SES-6	39172	2013-026A	June 3, 2013	1436.1	40.5° W
ARABSAT 1D (ANIK D2)	15383	1984-113B	November 8, 1984	1455.9	39.3° W
USA 252	39751	2014-027A	May 22, 2014	1436.1	38° W
TELSTAR 11N	34111	2009-009A	February 26, 2009	1436.1	37.6° W
NSS 10 (AMC-12)	28526	2005-003A	February 3, 2005	1436.1	37.5° W
EUTE 36A (EUTE W4)	26369	2000-028A	May 24, 2000	1462.4	36.7° W
GARUDA 1	26089	2000-011A	February 12, 2000	1441.2	36.7° W
ITALSAT 2	24208	1996-044A	August 8, 1996	1428.9	36.6° W
HISPASAT 36W-1	41942	2017-006A	January 28, 2017	1436.1	36° W
MARECS B2	15386	1984-114B	November 10, 1984	1501.1	35.6° W
THAICOM 1	22931	1993-078B	December 18, 1993	1451.8	35.2° W
INTELSAT 605	21653	1991-055A	August 14, 1991	1449.7	34.5° W
INTELSAT 35E	42818	2017-041A	July 5, 2017	1436.1	34.5° W
AURORA 2	21392	1991-037A	May 29, 1991	1454.3	34.4° W
OPS 6391 (FLTSATCOM 1)	10669	1978-016A	February 9, 1978	1454.5	34.2° W
SPACENET 3R	18951	1988-018A	March 11, 1988	1444.8	34.1° W

Figure 3. List of geostationary satellites orbiting (green) around Telstar-11N (red), easily misleading if the targeted spectrum is not known.

accurate aiming of the parabola to find the targeted signal (Fig. 4).

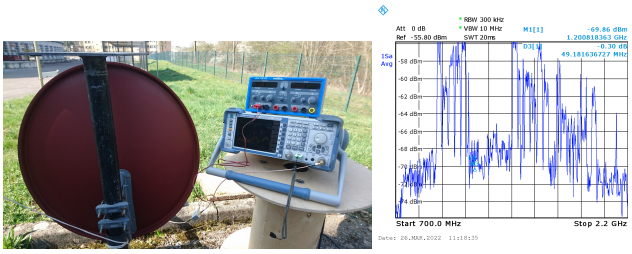

Figure 4. Left: searching for Telstar-11N signals by monitoring the spectrum of the signal collected by the parabola receiver coarsly aimed following the information provided by `https://www.dishpointer.com` but requiring fine tuning along the celestial equator to find the right satellite amongst the geostationary satellites. Right: example of one of the collected spectrum ... which happens not to be from the targeted satellite but a neighbor to Telstar-11N ! Indeed, no emission at the marker located at frequency offset 1.2 GHz is visible (see section 4).

4. Satellite links

Satellite television reception parabola have at some time in the past been a common sight on roofs to now become obsolete with terrestrial digital television broadcast (DVB-T, Fig. 5) or through optical fiber links. Many unused parabolas are hence available for experimenting, if we take the time to understand the operating conditions of the reception circuit located at the focal point, the LNB (Low Noise Block).

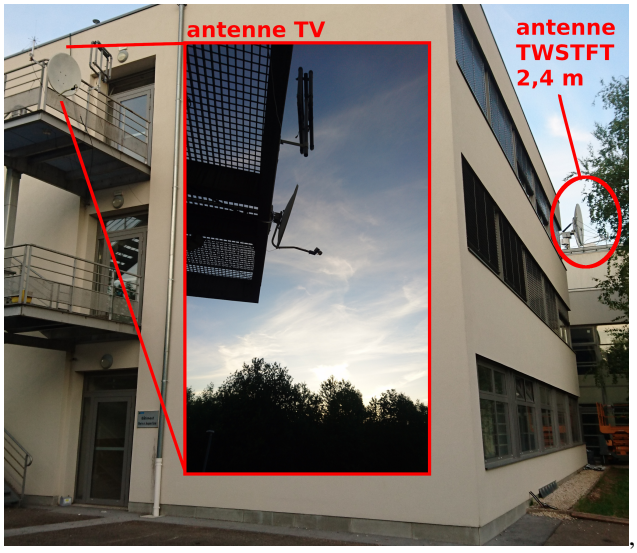

Figure 5. Experimental setup: a satellite television reception parabola (left) collects signals from Telstar-11N. Right, the 2.4 m diameter parabola dedicated to TWSTFT (Two Way Satellite Time and Frequency Transfer) of Time and Frequency Laboratory (LTFB) in Besançon (France), reference for validating results.

Despite its ridiculously low price, this set of electronic circuits provides two amplification stages (microwave and radiofrequenency), a local oscillator and a mixer for frequency transposition from the microwave range (10-15 GHz) to the radiofrequency band (1-3 GHz). The nominal frequency of the local oscillator is 9.75 GHz (Fig. 6) when powered through a bias-T (an inductor on the power supply and a DC-blocking capacitor towards the radiofrequency receiver) by a voltage between 13 and 18 V, the polarization of the receiving element rotating by 90° between these two voltages. Finally, injecting in the bias-T an audiofrequency signal at 22 kHz switches the local oscillator to 10.6 GHz, which will not be used here but might expand the operating frequency range of the LNB if needed, especially when considering the North American downlink frequency or for listening to the telemetry signals of the Starlink constellation satellites (10). We hence conclude that the Telstar-11N downlink frequency claimed by BIPM to be at 10953.95 MHz should be observed after frequency transposition by the LNB at 1204 MHz: this carrier frequency is the one to be set as local oscillator frequency of the software defined radio receiver connected to the LNB bias-T output.

The bias-T

The bias-T, described at https://www.youtube.com/watch?v=lxgpm-UXTNY, is a classical radiofrequency circuit allowing to share a common cable between two signals, one being the DC voltage to power the amplifier located as close as possible to the antenna, and the other radiofrequency signal carrying the information from the antenna to the receiver. These two signals must be split at both ends in order on the one hand to avoid wasting part of the radiofrequency (RF) signal in the power supply and on the other hand to avoid damaging the receiver by polarizing its input with a DC offset (which might happen by carelessly connecting the bias-T upside down: always check which port is DC-coupled and which port carries the sum of both DC and RF signals, since swapping these ports will probably damage the receiver frontend).

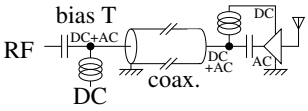

Principle of a bias-T at both ends of the coaxial cable, at right to the antenna and left to the receiver, carrying on its inner conductor core both the DC power supply and the RF signal. Both components are split at both ends by a bias-T made of a capacitor and an inductor whose value has been wisely selected (see text).

The bias-T locates an inductor (open radiofrequency circuit and DC short-circuit) between the power supply and the common midpoint, while a capacitor (open DC circuit and radiofrequency short-circuit) is inserted between the common midpoint and the receiver. Formally, the impedance of the capacitor $|Z| = 1/(C\omega)$ at angular frequency $\omega = 2\pi f$ at the operating frequency f is infinite if $f = 0$ and low if f is large, while the impedance of the inductor $|Z| = L\omega$ is null for the DC component at $f = 0$ and large when f increases. Practically, the inductor L and capacitor C are selected so that $L\omega \gg 1/(C\omega)$ and $1/(C\omega) \ll 50$ with $50\ \Omega$ the characteristic receiver impedance. If $f \gg 1$ GHz, any capacitor above a few nanofarads and inductor of a few microhenrys with match these conditions.

The software defined radio receiver is tuned to a nominal reception frequency of 1.204 GHz to collect the targeted signals, but due to LNB local oscillator fluctuations of a few hundreds of kHz to a few MHz and the restricted sampling rate of most software defined radio receivers insufficient to compensate for excessive local oscillator offsets after sampling, we might have to search for the signal a few hundred kHz on both sides of the nominal carrier frequency after transposition by the LNB.

Using a 60 cm parabolic reflector, the Telstar-11N signal is powerful enough to be easily measured above background noise, although a “real” broadband spectrum analyzer with 2 GHz bandwidth makes the search for the satellite signal

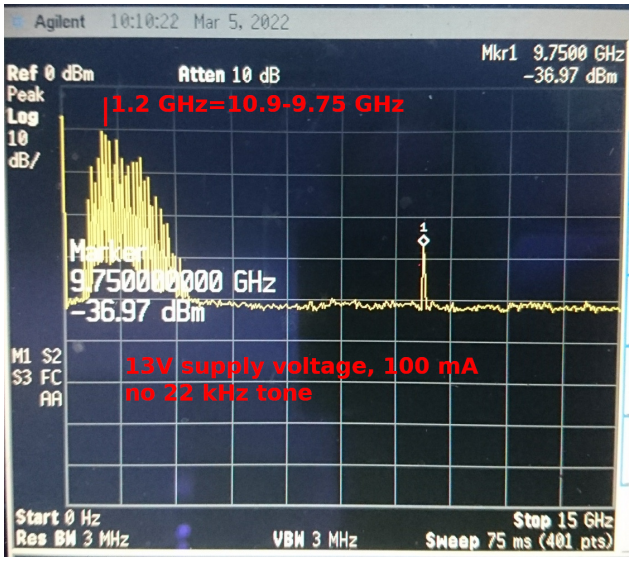

Figure 6. Spectrum analyzer measurement of the output of a LNB powered through a bias-T with 13 V (70 mA) as a source sweeps from 1 MHz to 10 GHz: the local oscillator leakage is clearly visible around 9.75 GHz while the band-pass filter of the LNB restrict the observed signals between 0.5 GHz and 2 GHz around this local oscillator frequency.

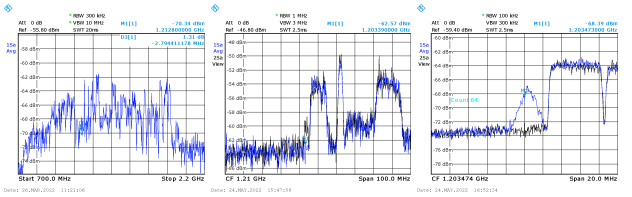

Figure 7. Spectra of signals broadcast by Telstar-11N with decreasing bandwidths from left to right, to finally focus (right) on the signals emitted by the modems of metrology Observatories, in blue during an emission and in black the noise floor when no signal is being broadcast.

much easier than just using the software defined radio receiver. Notice the powerful neighboring signal just above the signal we are interested in which is emitted continuously and much stronger (Fig. 7), making the search for the relevant part of the spectrum easier. Furthermore, we have learned that the signal bandwidth is 4.1 MHz and we will see later how sampling at 5 MS/s will make decoding easier: while the low cost RTL-SDR receivers exhibit insufficient bandwidth (2.4 MS/s only), we will use throughout this investigation the Ettus Research B210 receiver. We have however checked that a SDRPlay clone, the RSP1, is well suited for collecting an 8 MHz bandwidth after connecting the L-band input (1-2 GHz carrier signal) and decoding the time transfer signals, and many other receivers more affordable than the B210 and yet a bit more expensive than the RSP1 might be suitable as well (HackRF, PlutoSDR ...).

Parabola reflector size for satellite communications
Metrology laboratories, including the Time & Frequency laboratory in Besançon (France), are fitted with expensive 2.4-m diameter at least parabolic reflectors for their satellite link (Fig. 5). Why such complex and large installations when a simple 60 cm-diameter television reception parabola is sufficient? Gain is not the only relevant parameter of an antenna setup. The VSAT (Very Small Aperture Terminal) standard defines that when **emitting** from ground towards a satellite, only the targeted satellite must be illuminated and not its neighbors. Considering the density of satellites on the geostationary orbit, accurate aiming is mandatory, with an angular accuracy better than 0.5°. Considering that the beam emitted from an antenna is narrower as the antenna becomes larger, this emission regulation can only be met with a 2.4 m diameter parabola at least, with the additional benefit of the increased gain beyond the needs. Wikipedia justifies hence the rising operating frequency to shrink antenna dimensions while keeping narrow beams since `https://en.wikipedia.org/wiki/Ku_band` explains that "A major attraction of the band over lower frequency microwave bands is that the shorter wavelengths allow sufficient angular resolution to separate the signals of different communication satellites to be achieved with smaller terrestrial parabolic antennas." These aspects are detailed in the Very Small Aperture Terminals (VSAT) requirements published by Eutelsat at (12), much better documented than Telstar's information on these topics.

Having collected the data included in a spectral bandwidth matching the expected occupation – 4.1 MHz – we must check that the right signal has been collected: we can start by checking that this is indeed a binary phase shift keying BPSK modulation by plotting the spectrum of the squared signal. Indeed, a phase modulated signal $\varphi(t)$ but with a $\delta\omega$ frequency offset to the nominal carrier frequency programmed in the receiver local oscillator is expressed as $s(t) = \exp(j(\delta\omega t+\varphi))$ so that $s^2(t) = \exp(j(2\delta\omega t+2\varphi))$ and since for BPSK $\varphi(t) = \{0, \pi\}$ then $2\varphi = \{0, 2\pi\} = 0[2\pi]$ and the modulation spectrum spreading has been cancelled with all the signal energy collapsing in a pure carrier at $2\delta\omega$ on the spectrum (Fig. 8, left). The final proof that the right signals have been collected will come from decoding the payload by detecting the periodic correlation peaks between the transmitted pattern and the received signal (Fig. 8, right): the part is described in section 5.

Decoding the signals transmitted by the ground based radiomodems requires exactly compensating for the offset between the emitter local oscillator and the receiver local oscillator: Fig. 9 illustrates the proposed approach by con-

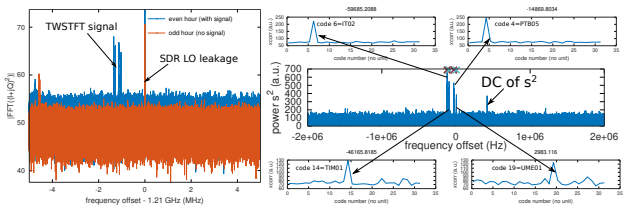

Figure 8. Left: spectrum of the squared signal during an emission (blue) within even UTC hour (14) and without emission (red) during an odd UTC hour. Right: for each carrier frequency offset, the correlation with a pattern transmitted by the SATRE modem is identified, demonstrating the proper understanding of the modulation scheme and its decoding.

sidering that each Observatory was allocated a known carrier frequency offset (13) and assuming that the pure unspread spectral component at lowest frequency offset after squaring the signal is from the Spanish ROA, we shift the spectrum along the frequency axis (multiplication of the signal with $\exp(j2\pi\delta f t)$ where δf is half the frequency offset observed on the squared signal with respect to its nominal value): we observe that when successful as seen on the three top curves, all Observatory signals align on their respective carriers, but sometimes excessive noise leads to a failure by identifying erroneously some noise component in the spectrum as the targeted signal (bottom). The final proof that the analyzed signal is the right one will come in the next section with decoding of the transmitted codes.

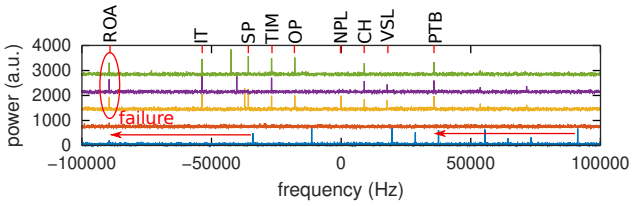

Figure 9. Alignment of the spectra to compensate for offsets between emitter and receiver local oscillators: we choose ROA as reference considering its pure spectral component after squaring the signal at lowest frequency is allocated to the Spanish emitter. The procedure was efficiently applied in the three top cases with all Observatories properly aligned on their respective frequencies, but failed when the targeted signal is absent (second from bottom) or if a noise in the spectrum was erroneously attributed to the Spanish carrier (bottom).

Finally we might wonder about the impact of replacing a 2.4 m parabola with a smaller 60 cm dish on the link budget. The emission, the satellite radiofrequency behavior and the downlink are not controlled in the context of this presentation, but it might be worth mentioning that the technical documentation of Telstar-11N at https://dokumen.tips/documents/telstar-11n-technical-manual-telesat-telstar-11n-te.html includes all the information needed to recover the link budgets described in the literature by depicting the parabolas on-board the satellite, and finally a convincing link budget is established by considering that the satellite acts as an amplifier with 100 dB gain (Fig. 10) in addition to shifting frequency from uplink to downlink carrier frequencies, assumption verified by varying the emitted power and observing that the received power varies similarly (acknowledgements to É. Meyer, Besançon Observatory, for this measurement report).

Finally, replacing the 2.4 m with 0.6 m reflecting parabola at the end of the communication link "only" induces as 12 dB loss on the receiving antenna gain which are easily compensated for with the flexibility of programming the software defined radio receiver.

5. Decoding timing signals

Identifying the pseudo-random sequence code in CDMA communication has been widely addressed, for example after the launch of the first European Galileo satellite whose code was supposed to remain secret but was quickly reverse engineered (15). The problem will be much simpler in this case.

Le file collected on the BIPM web site previously informs in the MODEM field that the transferred signals were generated thanks to a SATRE (Satellite Time and Ranging Equipment) instrument sold by the German TimeTech company. As all commercial product, no documentation on the internal operation or the proprietary communication protocol is available. Looking through history though tells us that TimeTech acquired the technology as developed under the name MITREX in the 1980s in Stuttgart (Fig. 11), and a few German, Dutch and Japanese articles superficially describe the internal operations of this modem: we will assume that the private company has kept all the scientific underlying principles to only add a cosmetic shine and the applicative layer of slow digital communication which will hardly be addressed in this document.

Indeed, we learn in (16; 17; 18) that the authors of MITREX have used a 14-bit long pseudo-random sequence code truncated to 10000 elements (chips) to be easily multiple of a power of 10, and that this code is transmitted every even universal time UTC hour (14). Not only is the datarate deduced by observing the spectra of the received signal and noticing that the first null on both sides of the carrier of a BPSK modulated signal are located at the datarate, here 2.5 MHz and hence 2.5 Mb/s, but also by the fact that the autocorrelation of the signal exhibits peaks every 4 ms, length of the code after which it repeats ($2.5 \cdot 10^6 \times 4 \cdot 10^{-3} = 10000$). This short repetition rate

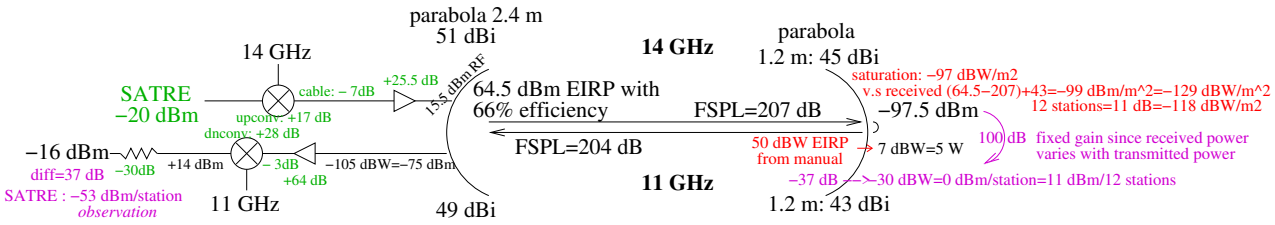

Figure 10. Link budget with the assumption that the satellite acts as a 100 dB amplifier in addition to frequency transposition from uplink to downlink carrier frequencies.

These constraints have been met by the MITREX MODEM. It is an interface between the 70-MHz IF of a standard earth station, a Time Interval Counter TIC and the time keeping hardware, i.e. the atomic clock. The hardware is housed in a 19-inch drawer and operates as a pseudorandom noise sequence (PN) encoder/decoder of the time signal. The PN-code is a truncated maximum length sequence of period 10.000, instead of the 16.383 chips. This period of 10.000 eases the overall system design, as it allows the use of even and decimal dividers for signal processing. The correlation features of the maximum length sequence are almost retained.

2.2 PN-Encoding/Decoding

Figure 11. Excerpt of the article by Hartl (16) justifying the knowledge of the length of the code used by SATRE.

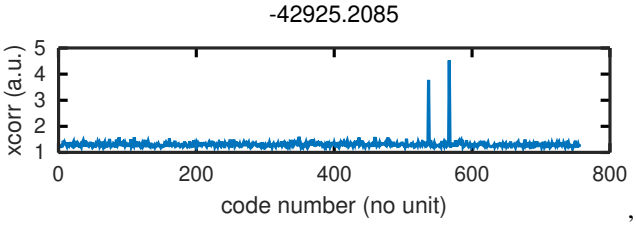

Figure 12. Correlation with all possible 14-bit long codes truncated to 10000 chips: notice that two codes exhibit significant correlation, hinting at a questionable orthogonality if the selected subset of possible codes has not been carefully selected.

induces an uncertainty on the absolute time of flight since, remember, it is in the order of 240 ms from ground to the geostationary satellite and back to ground.

Although fancy ways of generating such sequences that never repeat such as the GPS L1 Gold codes, the most intuitive approach (19) is the Linear Feedback Shift Register (LFSR) in which a shift register is fed each new clock cycle a combination of exclusive OR (XOR) of some values located within the register at the so-called taps. An exhaustive search using this method is not computationally challenging since https://users.ece.cmu.edu/~koopman/lfsr/ tells us that "only" 756 possible means of generating the $2^{14} - 1$ long codes that never repeat exist, and even not knowing the starting point of the truncation of the sequence to 10000 elements, the 16383 long sequence will still exhibit a 61% overlap for a well defined correlation peak to appear if the right sequence is used (Fig. 12). Since the initial value of all 0s is forbidden (XOR(0,0)=0 so the code would always remain 0), we can assume that a starting point will all 1s, or 0x3FF, is an obvious selection. We are left with identifying the pseudo random sequence formalism between Fibonacci and Galois algorithms which both provide the same sequence but with a time offset. This analysis will not be developed further here but is described in detail at https://github.com/oscimp/gr-satre for the reader willing to reproduce the investigation.

Finally, asking Google for a search on "satre modem manual" leads as second link (depending on the cookies the browser has accumulated) to a file transfer site ftp://ftp.npl.co.uk/npl/twstft/ which happens to leak all information needed to generate the pseudo-random sequences. We have saved in https://github.com/oscimp/gr-satre/blob/main/taps.txt the 10000 binary chip long sequences matching each ground based emitting station pseudo-random code.

Decoding the signal is finally summarized as

1. compute the square of the received signal to evaluate the offset between the carrier frequency of each emitter and the receiver. Although the emitters of all metrology laboratories are clocked by frequency references whose accuracy is (by definition) perfect and the offset is mainly due to the LNB, we observe that the satellite frequency transposition is partly a cause of frequency offset when shifting from the 14 GHz uplink to the 11 GHz downlink, and furthermore each

Observatory has been attributed a unique frequency offset of a few kHz to improve correlation orthogonality (13)

2. for each identified carrier frequency offset δf, digitally compensate by mixing with a numerically controlled oscillator $\exp(j2\pi\delta f t)$ to center the carrier on 0 Hz and correlate with all possible codes. The value of δf results from a Fast Fourier Transform on N samples sampled at a rate f_s so that the frequency resolution is f_s/N. Considering the code is 10000 chips long, the transmitted signal at $f_r = 2.5$ Msamples/s as assessed by the first two nulls at ± 2.5 MHz on the received signal spectra means that the transmission duration of each sequence is 4 ms so that the δf must be identified with an accuracy better than 1000/4=250 Hz to make sure the energy accumulation condition is met when correlating without wasting energy on an excessive left-over frequency offset whose mean value would be null. For a sampling rate of $f_s = 5$ MS/s spanning the whole transmission band and yet being compatible with the datarate of the B210, we conclude that $N \gg 5 \cdot 10^6/250 = 20000$. Practically, we will select N in the few hundred thousand samples range,

3. correlations are computed on 20000-long IQ sample sequences collected at a sampling rate of 5 Msamples/s ($20000 = 5 \cdot 10^6 \times 4 \cdot 10^{-3}$), making sure a unique correlation peak is found in this interval if the emitter matching the searched sequence is active

4. finally, the correlation peak identified with 200 ns steps (inverse of the 5 MHz sampling frequency) is fitted with a parabola expressed as $at^2 + bt + c$ with a summit and both neighbors on both sides as correlation peak maximum, with its exact maximum location positioned at $t_0 - b/(2a)$ with t_0 the abscissa (integer) of the correlation peak: the fractional correction $-b/(2a)$ is as accurate as the signal to noise ratio for determining a and b.

5. Searching for the correlation peak is repeated on the whole measurement sequence and a mean value is deduced after parabolic fitting of the delays to compensate for the drift of the satellite along its orbit.

This last step is a core element for improving the timing resolution from the sampling period of 200 ns to the targeted few nanoseconds: we can demonstrate that under the assumption of a single correlation peak, the improvement on the timing resolution as the maximum of the correlation peak location is equal to the measurement signal to noise ratio (20). This approach is commonly used for sub-pixel motion measurement in image processing.

Fig. 13 generalizes these considerations by testing all possible pseudo-random codes with all possible frequency offsets – this calculation could have been simplified by restricting frequency offsets to those found by squaring the signal (Fig. 9). The 1800 Hz frequency offset of each carrier to the nominal value is introduced by the geostationary satellite frequency transposition.

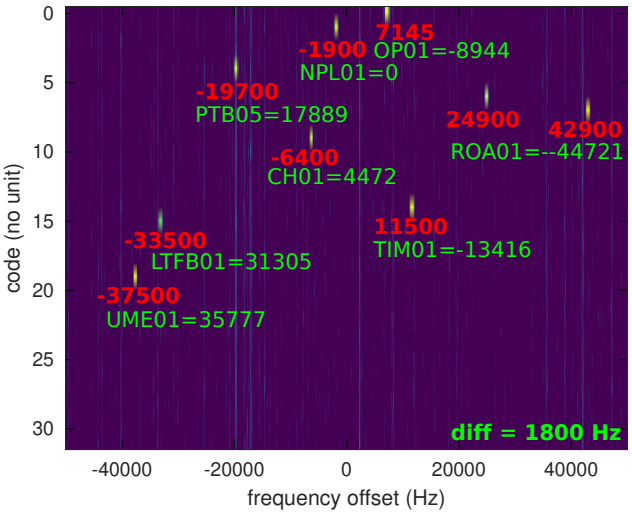

Figure 13. Map of all possible codes (Y-axus) for all possible frequency offsets (X-axis) as would be classically displayed when analyzing GPS signals or ambiguity functions in general, except here the frequency offset is defined by the emitter and remains constant from one emission to another as opposed to a continuous variation induced by a Doppler shift.

6. Digital messages transmitted by SATRE modems

Now that we have identified the correlation peaks separated every 4 ms or 10000 chips at a rate of 2.5 Msamples/s, have we extracted all the possible information from the transmitted signals? If we consider GPS (21), we know that the navigation messages are overlaid at a rate of 50 bits/second above the code identifying which satellite is broadcasting at a rate of one correlation every millisecond. Hence, 20 successive correlations represent the value of one navigation bit, with a correlation equal to either +1 or -1 depending whether the transmitted message bit is 1 or 0.

TimeTech does not document such a functionality of the SATRE which is also never mentioned in MITREX related publications, but the manual (Fig. 14) leads us to believe that a digital communication layer exists above the time transfer code. Since we have identified the correlation phase by compensating for the frequency offset between local oscillators of the emitter and receiver, we can investigate the sign of the resulting phase to deduce the

In addition the master provides via HiRate data all necessary information to enable calculation of the predicted arrival time (PAT) at the satellite by remote modems receiving the ranging signal:

$$PAT = PathA + TxDelay_A - ClockOffset_A$$

A pseudo-ranger calculates it's own 2-way range in the following manner:

$$t_{RB} = t_{TA} + TxDelay_A + PathA + PathB + RxDelay_B$$
$$Raw_B = t_{RB} - t_{TB} =$$
$$= TxDelay_A + PathA + PathB + RxDelay_B + (t_{TA} - t_{TB}) =$$
$$= TxDelay_A + PathA + PathB + RxDelay_B + ClockOffset_B - ClockOffset_A$$
$$PathB = Raw - RxDelay_B - PAT - ClockOffset_B$$
$$Range = 2 \times PathB$$

,

Figure 14. Excerpt of the SATRE modem manual mentioning the digital communication never described in any publication (17) a whose encoding is obviously never documented. TimeTech has indeed added a communication protocol above the MITREX time distribution layer, but is not disclosing its organization.

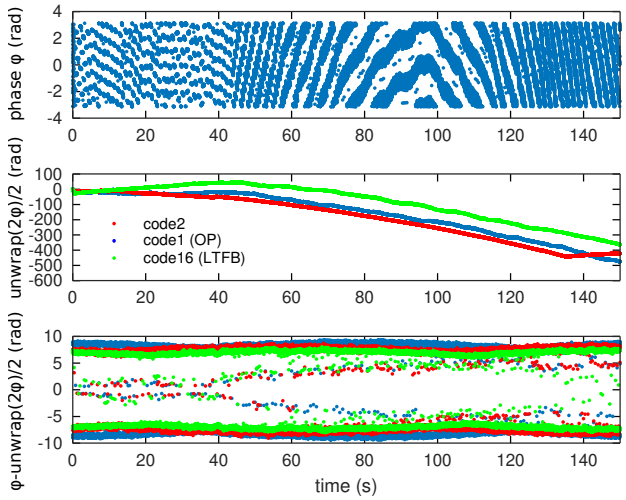

Figure 15. Unwrapping the phase (top) by subtracting half the phase of the squared signal (middle) to only keep the BPSK modulation carrying the digital information overlaid on top of the code of each broadcasting station (bottom).

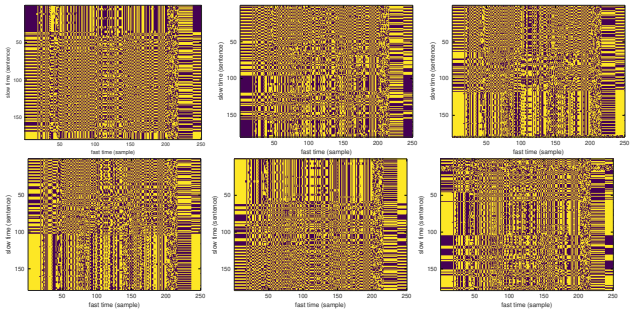

Figure 16. Evolution of each 250 bit long sequence (X-axis) lasting 1 second, sentence after sentence (Y-axis) to visualize patterns that might repeat from one sentence to the next, allowing to identify some field in the digital communication sentences shared by the modems. From left to right and from top to bottom the investigation of modems transmitting codes 15, 1, 16, 10, 2 and 4.

transmitted but value. Indeed, subtracting the to the phase of the received signal half the phase of the squared signal (Fig. 15), we recover only the modulation term used for transmitting the digital payload in addition to the code: $\Phi = \varphi - unwrap(2\varphi)/2$ is equal to $\exp(j0)/\exp(j\pi)$ i.e. $\pm 1 \in \mathbb{R}$ which encodes the to possible transmitted bit states. Thus, for SATRE (Fig. 14) the story happens to be the same than for GPS, without the redundancy and with a higher datarate allowed by the more favorable link budget. Alternatively, if instead of looking for the magnitude of the correlation peak we were to investigate its real part, we expect the digital code to appear thanks to the linearity of the correlation, and it would be quite intuitive to expect this code to be transmitted at a rate of about 250 bits/second, inverse of the 4 ms period of the correlation peaks. We check that indeed using an autocorrelation on the digital sentences that peaks appear at multiples of 250 samples, signature of some pattern repeating at this rate.

Indeed by reorganizing each time series of the correlation peaks as matrices with 250 columns (fast time axis) and as many lines as allowed by the length of the processed sequence (slow time axis along which messages are expected to repeat), we observe some repeated patterns (Fig. 16) hinting at digital messages.

If as we might expect one of the fields is the time in seconds, we would expect the least significant bit to alternate between 0 and 1 every second whether it is odd or even, and the next bit alternate once every two lines, but nothing that trivial appears when observing these patterns. A forward error correcting code could be used to correct for communication errors, but no such encoding is detected with an investigation as described in (22) implemented with `https://github.com/BatchDrake/cccrack`. Although we have not investigated further in this direction, the alternating color of the first columns which appear constant otherwise hint at a differential binary phase shift keying which indeed leads to consistent repeated pattern from one line to the next. We now focus on investigating further processing of timing signals as the core topic of this presentation, leaving the digital communication layer for further investigation.

7. Time transfer: observing timing signals shared during two-way links

Fig. 17 illustrates the evolution of the time offsets differences between correlation peaks associated with each Observatory, with an additional artificial offset introduced to better separate the various curves. Since the various European Observatories do not see the satellite with the ex-

act same line of sight, the projection of the velocity vector of the satellite moving around its equilibrium point due to gravity forces (Moon, Sun, non-spherical shape of the Earth) differs for each Observatory and the residual motion is observed. Each Observatory communicating with its neighbors is sharing ranging information between itself and the satellite, as well as the time of flight between itself and the other speaker. Thanks to these two information the absolute time at both sites can be deduced. These are the information collected by the BIPM and shared on the file server mentioned earlier, and we observe an excellent match between our own observations and the values published by BIPM, for example when comparing the delay difference between Paris Observatory and the Spanish ROA on Fig. 17 (top), blue being our observations and purple being the measurements shared by BIPM.

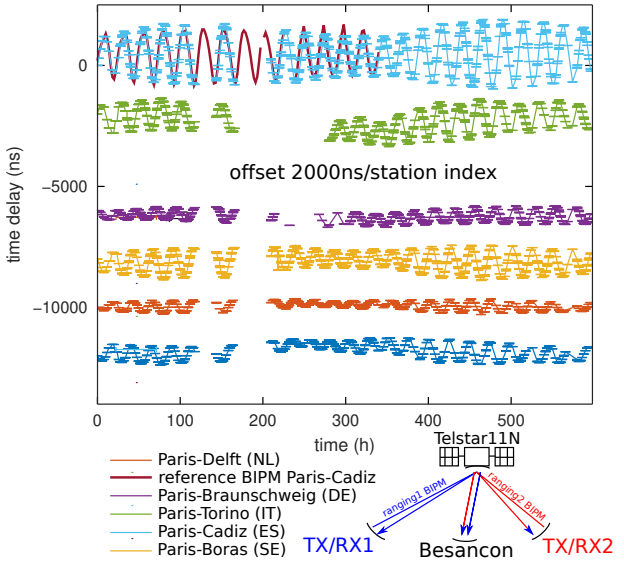

Figure 17. Time offset between the correlation peaks associated with each European observatory communicating through Telstar-11N: the motion of the satellite is clearly visible, each Observatory being assumed at a fixed location and transmitting a timing signal assumed to be "perfect".

A subtlety remains to reach such an excellent agreement. While software defined radio receivers we are using allow for processing the signals from all Observatories simultaneously – we have recorded the whole bandwidth as IQ samples in the 5 MHz frequency range around the carrier during the whole link duration – the antique SATRE can only process two stations at any given time, and the exchanges between all Observatories require sequential communication between speakers only able to talk two by two at any given time. Such sequential communication induces some delay between the measurements collected by BIPM which must be compensated for when comparing with SDR records: we indeed observe on these charts that the satellite is moving at a rate of a few nanoseconds every second (remember that light propagates at 30 cm/ns so that a few nanoseconds every second mean a velocity of a few meters per second), and hence some delay of about 10 minutes between two observations quickly lead to a few microsecond offsets between measurements. Only by interpolating measurements published by BIPM to interpolate at the same measurement time – in our case a linear interpolation is enough considering the slow motion of the satellite – can the excellent match be achieved as illustrated on Fig. 18. Without such an interpolation, the delays reach well beyond a few microseconds between BIPM data and our observation, a disagreement that cannot be overlooked considering the targeted resolution of a few nanoseconds.

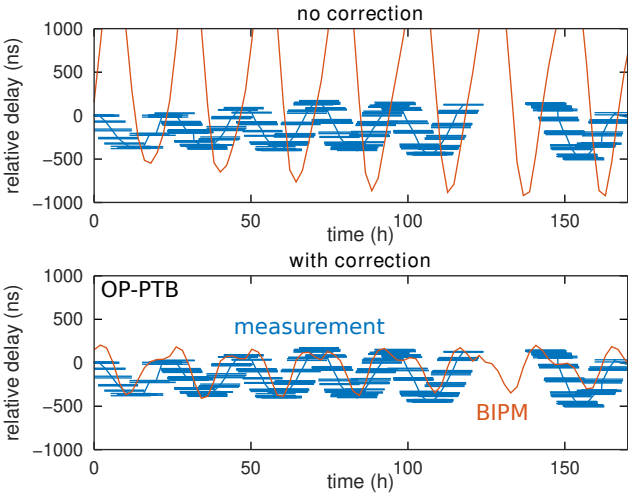

Figure 18. Comparison of the measurements published by BIPM (red) and our observations using SDR (blue) without interpolation of the measurement times (top) and with the correction by linear interpolation of the measurement dates (bottom). Only in the latter case is the match excellent.

We are now convinced we are able to decode the timing signal broadcast by European Observatories and identify the time delay between their emissions considering the motion of the satellite. Can we benefit from this knowledge to control a local clock with a purely passive, without a two-way link, just by observing the signal shared daily. The challenge lies in the motion of the satellite, since the information collected by BIPM and shared on their web site would allow correcting the varying distance from Observatory to the satellite after the measurement completion, but the common term from satellite to the ground station is not controlled (Fig. 17, bottom). This is the term we need to try and identify to subtract its contribution.

8. Time transfer: observing timing signals for one-way correction

```
x1=300 % 3 m ou 1500 km
x=0;x2=0;z1=0;z2=0;z0=0
v=3e8
z=36000e3  % 36000 km
p=1
for x=[0 30000] % 30 km
  r1=sqrt((x-x1)^2+(z-z1)^2);
  r2=sqrt((x-x2)^2+(z-z2)^2);
  dt(p)=(r1-r2)/v;
  p++;
end
diff(dt)
```

Figure 19. GNU Octave simulation code of the time of flight as the satellite is moved around its equilibrium position.

The first approach that comes to mind to compensate for the satellite motion is to observe with multiple ground based parabolas close to the reception site and analyze the phase to detect and compensate for this motion. This approach, reminiscent of the classical radiofrequency Direction of Arrival (DoA) processing or Synthetic Aperture RADAR (SAR), however appears challenging: a satellite 36000 km away moves by about 30 km around its equilibrium point. Two antennas located 3 m apart when considering a reasonable baseline will detect signal shifted in time by only a few picoseconds, impossible to measure considering the available bandwidth, and the antennas must be spaced by more than 300 m to reach the hundreds of ps of time of flight difference, within the standard deviation of the correlation peak delay measurement but harder to implement experimentally (Fig. 19). The conclusion that the longer the baseline, the larger the delay difference induced by the satellite or start motion and the easier it will be to measure, is the basics of distributing radiotelescopes on as large as baseline as possible, reaching sometimes across continents.

In our case, we can then take the problem the other way around by considering that multiple observatories are transmitting signals assumed to be synchronous and coherent, and that the unique observer (us) can benefit from this spatial diversity of the sources to recover the position of the satellite and hence compensate for its variation, knowing the exact coordinates of all emitting sites. This approach has been described in (23) without addressing the technical challenges beyond promising results.

We can start by being convinced of the need to measure and compensate for the delay induced by the satellite motion by timestamping the correlation peaks with respect to a local time reference, for example provided by the 1-PPS pulse of the U-Blox GPS receiver. Indeed as in the problem we are interested in here, each satellite of the GPS constellation emits a timing signal supposedly synchronous and the trilateration at the ground receiver allows for compensating the time of flight of the electromagnetic wave and recover the location of the receiver. This 1-PPS every second is assumed stable over time since it is generated by atomic clocks embedded in the satellites and monitored daily by the American USNO to make sure of their accuracy (after broadcasting corrections in the navigation messages). Fig. 20 illustrates the evolution of the time at which the correlation peaks are recorded as observed in Besançon for emission from European Observatories: to obtain such a result, the B210 software defined radio receiver was configured to trigger its acquisition on the rising edge of the 1-PPS signal of a GPS receiver. Such a result is achieved by editing the GNU Radio Companion acquisition script and adding the command after the connection of the various processing blocks (first two lines generated by GNU Radio Companion, our additions below):

```
self.connect((self.blocks_head_0, 0), (→
    ↪self.blocks_file_sink_0, 0))
self.connect((self.uhd_usrp_source_0, 0),→
    ↪ (self.blocks_head_0, 0))
# add external 1-PPS trigger:
curr_hw_time = self.uhd_usrp_source_0.→
    ↪get_time_last_pps()
self.uhd_usrp_source_0.set_time_next_pps(→
    ↪ uhd.time_spec_t(0.5) + curr_hw_time→
    ↪)
time.sleep(0.1) # must be << 1 s
self.uhd_usrp_source_0.set_start_time(uhd→
    ↪.time_spec_t(1.01) + curr_hw_time)
```

which tells the UHD library controlling for GNU Radio the B210 to wait the next rising edge of the PPS signal before launching the acquisition. We observe on Fig. 20 that the timestamp of the correlation peaks fluctuates from one day to another by more than 150 μs, or a satellite motion amplitude of about $0,3$ km/μs $\times 150$ μs $= 45$ km, well within the expected variations considering known orbital parameters. However, synchronizing clocks within 150 μs accuracy would be a performance worse than those obtained when synchronizing with the very low frequency signal emitted from Mainflingen at 77.5 kHz (DCF77 "radiocontrolled" clocks) (24) and insufficient to meet the compliance requirements of the MiFID2 European standard that requires timestamping financial transactions with sub-100 μs accuracy.

We now have two options: predict the satellite motion or observe the satellite motion, in both cases with the objective of correcting the impact of its position and compensating for the variation of the time of flight of the electromagnetic waves from emitter-satellite-receiver, both ends of the link being assumed at a fixed location. Neither of the two solutions is trivial and let us alert the reader right now that none will reach an acceptable solution, even if the fact of just observing the motion of the satellite at a range of 36000 km from the receiver already seems incredible.

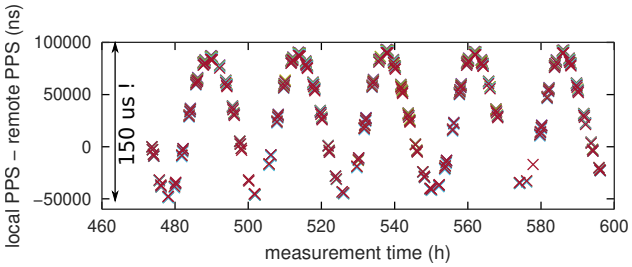

Figure 20. Evolution of the timestamp of the correlation peaks from one European Observatory with respect to the GPS controlled 1-PPS, illustrating the motion of the satellite around its equilibrium point by about 45 km.

8.1. Analysis of predicting the position of the satellite

Knowing that the satellite orbital parameters are documented as TLE (Two Line Elements) published by the NORAD and that tools for predicting satellite position such as (RIP) SatTrack, Gpredict, `previsat` or the Python `skyfield` library (25) are available, we might consider predicting the position of the satellite in space and hence compensate for the time of flight of the electromagnetic wave. While the calculation of Low Earth Orbiting satellite trajectory allows to predict within a second the time at which weather satellites or the International Space Station ISS rises or sets, we have discovered that the status is much more complex in the case of geostationary orbiting objects (26) which require different means of finding the solution, or even for which the TLE indicating eccentricity and the number of orbits per day are just not suitable. With a TLE expressed as

```
1 34111U 09009A   22108.22260583 -.00000247  00000+0  00000+0 0  9991
2 34111   0.0138 228.2697 0001723 157.0655 223.5808  1.00270830 48160
```

we can clearly see that the number of orbits per day (1.00270830) or the fractional part of the eccentricity (0001723) will suffer from an insufficient number of decimals to feed the SGP4 algorithm implemented to search for the solution as confirmed at `https://rhodesmill.org/skyfield/earth-satellites.html` which cites (27)

> "The maximum accuracy for a TLE is limited by the number of decimal places in each field. In general, TLE data is accurate to about a kilometer or so at epoch and it quickly degrades."

and complemented with

> Satellite elements go rapidly out of date. You will want to pay attention to the "epoch" – the date on which an element set is most accurate — of every TLE element set you use. Elements are only useful for a week or two on either side of the epoch date. For later dates, you will want to download a fresh set of elements. For earlier dates, you will want to pull an old TLE from the archives.
> Expect a satellite's orbit to constantly change as the SGP4 propagation routine models effects like atmospheric drag and the Moon's gravity. In particular, the true anomaly parameter can swing wildly for satellites with nearly circular orbits, because the reference point from which true anomaly is measured – the satellite's perigee — can be moved by even slight perturbations to the orbit

Hence, (27) warns that it would be deceptive to try and search for the location of a celestial object to better than a few kilometers, or in our case an uncertainty of a few tens of microseconds. This observation does not call into question the ability of TLE to accurately predict the date at which a low Earth orbiting rises or sets: the International Space Station (a NOAA weather satellite) at an altitude of 400 km (850 km) travels its 43000 km-long (46000 km) orbit in 93 minutes (101 minutes) so that an error of 10 km on the location only shifts by 1.3 seconds the rise or setting time over the horizon, scarcely detectable for a flight from horizon to horizon lasting around 6 minutes (11 minutes).

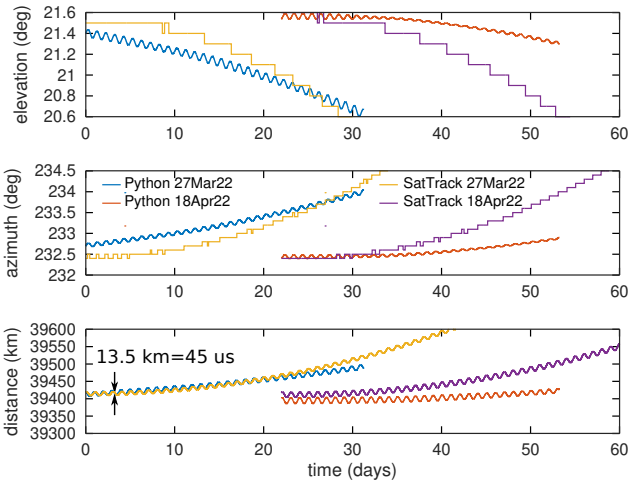

Figure 21. Comparison of the solutions provided by SatTrack and Python's SkyField for two identical starting conditions and a prediction to 1 month of the location of the satellite in space. While Skyfield exhibits at least daily orbital fluctuations, SatTrack lacks resolution and diverges quickly.

In order to further investigate the feasibility of this approach though, T.S. Kelso from Celestrak has kindly provided the TLEs from Jan. 1st 2022 to Apr. 18 2022, and

we have attempted to investigate how far in the future the satellite position could be predicted and at what point the solution starts diverging. Let us start by immediately eliminating the SatTrack option (Fig. 21) which although being able to provide a solution, quickly diverges and does not provide enough decimals to even observe the daily position fluctuations. We have hence focused on `skyfield` which appears best suited to our objective:

```
from skyfield.api import load, Loader, →
    ↪EarthSatellite
from skyfield.api import N,S,E,W, wgs84
from skyfield.timelib import Time
import numpy as np
import csv

load =Loader('./')
data =load('de421.bsp')
ts   =load.timescale()
earth=data['earth']
lab  =wgs84.latlon(+47.0*N, +6.0*E,→
    ↪elevation_m=143)
sat_tle = load.tle_file('sat34111.txt')  →
    ↪# lecture du fichier de TLE
for k in range(0,len(sat_tle)):
    print(sat_tle[k].epoch.utc_jpl()+" = →
        ↪"+sat_tle[k].epoch.utc_strftime(→
        ↪'%s'))
    hours = np.arange(int(sat_tle[k].→
        ↪epoch.utc_strftime('%H'))-1, →
        ↪24*8, 0.1)
    diff=sat_tle[k]-lab
    time = ts.utc(int(sat_tle[k].epoch.→
        ↪utc_strftime('%Y')),int(sat_tle[→
        ↪k].epoch.utc_strftime('%m')),int→
        ↪(sat_tle[k].epoch.utc_strftime('→
        ↪%d')), hours)
    topocentric=diff.at(time)
    alt, az, distance = topocentric.altaz→
        ↪()
    nom="res"+sat_tle[k].epoch.→
        ↪utc_strftime('%s');
    with open(nom, 'w', newline='') as →
        ↪csvfile:
        o=csv.writer(csvfile, delimiter='→
            ↪ ', quotechar='|', quoting=→
            ↪csv.QUOTE_MINIMAL)
        o.writerows((distance.km,alt.→
            ↪degrees,az.degrees))
```

This script defines the observation location (`lab` located in Besançon at 6°E and 47°N) and then for each entry of the orbital parameters of the satellite in the file `sat34111.txt`, we calculate {azimuth, elevation, distance} of the satellite using `topocentric.altaz()` whose result was saved in a file for post-processing. Although the general trend of the daily fluctuations of the satellite position are well visible (Figs. 22, 23), attempting to predict the position of the satellite on an 8-day horizon is already challenging (Fig. 22) when the solution does not outright diverges, even on as short a delay as 1 day (Fig. 23).

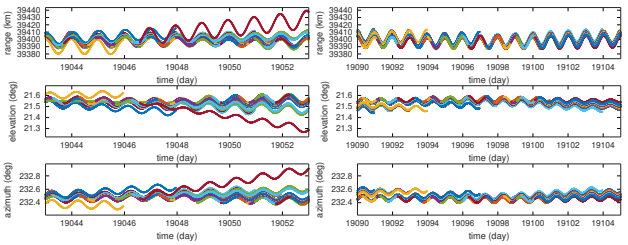

Figure 22. Long term prediction sequences illustrating the divergence of the solution and emphasizing the need to regularly update TLEs.

This approach hence seems doomed to failure, or at least with the simple tools available to us and easily accessible as described here. C. Rieck (23) mentions describing the orbit "by a GPS ICD [7] compatible Kepler model, which is estimated using iterative nonlinear least squares" which we have no clue how to use, while these authors further indicate that the geostationary satellite position is regularly fine tuned to keep it within the volume that it was allocated over the equator, corrections which cannot be predicted but only observed.

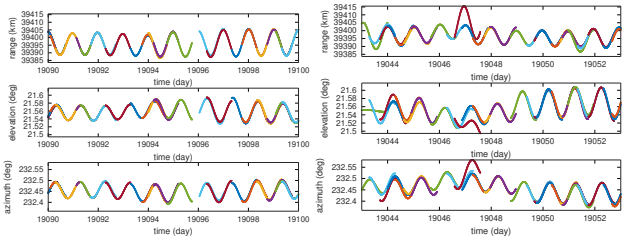

Figure 23. Zoom on a short term prediction sequence, left in a well behaved case, when the prediction indeed matches the evolution of the orbit updated with new TLEs, and right in the case of a divergence when new TLEs must be quickly updated to further complete the calculation.

8.2. Analysis of observing the satellite position

We have seen that the spatial diversity of the emitters should allow, thanks to a long enough baseline, to separate the various projection of the components of the satellite motion vector onto the vectors linking the satellite to each ground station, and hence identify each component. With 8 observatories distributed on the European continent (Fig. 2), the solution is over-constrained and we should consider a least-square optimization solution, but since practically all Observatories are grouped in close locations with respect to the satellite we shall try to favor the widest baselines provided by the Swedish station SP, the Spanish ROA, the British NPL and the Italians at INRIM (Fig. 24). The map of Fig. 2 illustrates how poorly conditioned the problem is, with a satellite eccentrated since it is used for also communicating with North America, and hence is seen at

roughly the same direction from all locations in Europe.

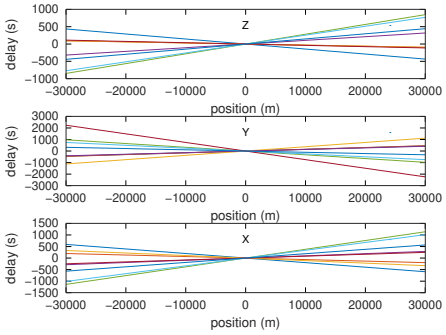

Figure 24. Prediction of the impact according to a simple geometrical model of the delay of the signal (Y-axis) with the variation of the position X, Y or Z of the satellite around its equilibrium point, as seen by the various Observatories located in Europe (array of lines with different colors). The aim of processing the received signal is the opposite, namely finding the location of the satellite (X, Y, Z) which best matches the observed communication delays as observed on a ground station.

Having analyzed the direct problem, namely identifying the delay of a few hundreds of nanoseconds to microseconds induced by the time of flight from each Observatory due to the motion of the satellite along the three axis in Cartesian coordinates (Fig. 24), the most naive approach but easiest to implement is a gradient descent search of the optimal solution: we express the problem by evaluating the time delay introduced in a communication link between the satellite whose position is free to be adjusted and each Observatory whose location is known, and ask GNU/Octave to minimize the residual error of the observed and predicted delays by wisely selecting the position of the satellite. Practically, this approach is extremely sensitive to noise and leads to hardly credible results. Indeed the result is disappointing and fails to converge, especially with a strong dependency with the the number of Observatories included in the analysis, signature of an excessive sensitivity to measurement noise (Fig. 25): the general conclusion is that this method should be implemented as a Kalman filter, method that we are not (yet!) able to understand.

The alternative to a gradient descent is an exhaustive search of the optimal solution by sweeping the whole space of possible solutions. We consider a cube with 200 km edges centered on the nominal position of the satellite and discretized with 3.9 km steps (13 μs which would already be a huge delay but selected to keep computation time reasonable) and compute the delay introduced when each Observatory is communicating with the satellite, and for each position consider the sum of the square of the differences between measurements and estimates: hence the most probable solution appears as a minimum error function in the maps. Consider the computation time involved, the maps

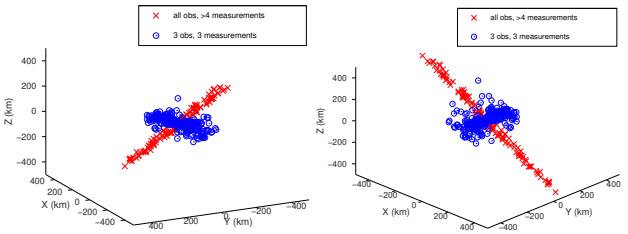

Figure 25. Gradient descent solution of the position of the satellite around its equilibrium point assumed to be 36000 km over the equator at longitude -37.5° depending whether all delays measured by at least four European Observatories are considered (red), or only the three most eccentric (blue).

are only estimated on the horizontal plane ($Z = 0$) and vertical planes ($X = 0$ and $Y = 0$) and not in the whole volume of the cube (Fig. 26). Fig. 27 illustrates some of the results of this investigation over a bit less than a month, less incredible than the gradient descent but still excessively noisy which would not allow recovering the satellite position with enough accuracy to compensate for varying times of flight.

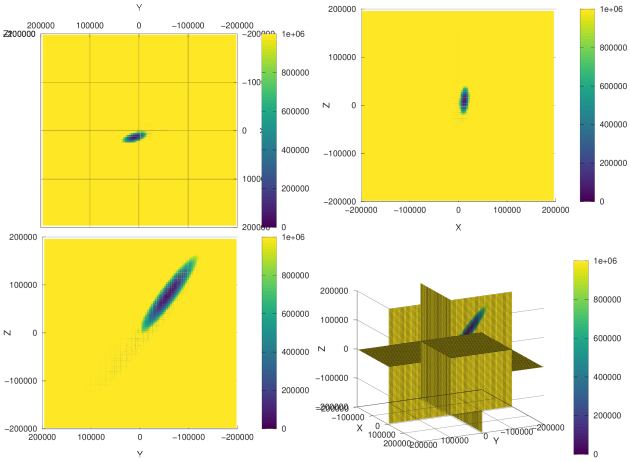

Figure 26. An example of an observation at a given date of the map of the error function deduced by adding the squares of the differences between calculated and observed times of flight as a function of position of the satellite swept on each point of the horizontal and vertical planes (all axis graduated in meters). A minimum is observed in each plane but the 3D view bottom right emphasizes how poorly conditioned the problem is along the radial Z axis of the satellite position.

9. Conclusion

We have started this exploration of radiofrequency communication links with a geostationary satellite by aiming to decode signals shared between European Observatories for comparing their reference clocks. Doing so, we have discovered how LNBs operate at the focal point of parabola

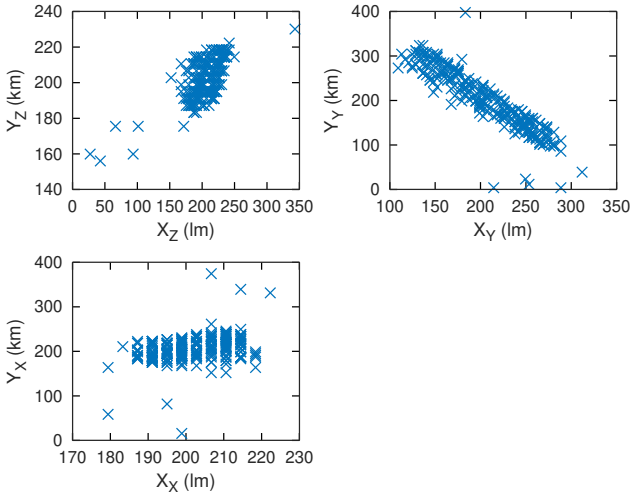

Figure 27. Evolution of the position of the minimum of the cost function indicating the most probable solution during the 200 successive measurements collected over 20 days. The results are too noisy to allow retrieving the satellite position and compensate for the electromagnetic wave time of flight propagation variation due to its motions.

reflectors in order to amplify and frequency shift the downlink signal to feed a software defined radio. Thanks to sufficient bandwidth, we have explored the binary phase shift keying BPSK modulation to identify orthogonal pseudo-random codes transmitted by each Observatory, and hence recover the time of flight between each Observatory and the unique receiver: this measurement allows for observing the oscillations of the geostationary satellite around its equilibrium point, but most significantly deduce from the time interval between the correlation peaks the frequency instability of the local oscillator in order to later correct it. Having attempted to predict the motion of the satellite preventing the accurate time information recovery on the ground, we have focused on observing this motion. The noisy measurements do not allow for finely recovering the location of the satellite in space in order to compensate for time of flight variation, which will always remain polluted with ionospheric and tropospheric delays between the satellite and the receiver which cannot be observed. Many technical challenges requiring a broad range of competencies remain to be solved to provide a readily usable solution for controlling clocks on the metrological signals transmitted by European and North American Observatories.

It is usually frowned upon to add a new information in the conclusion but how come we have spent the whole document discussing time and frequency transfer using correlation peaks and not the signals correcting the local oscillators as would be usually done in a ground-based radiofrequency link? The problem lies in the satellite which appears as a black box whose operation is not controlled: the

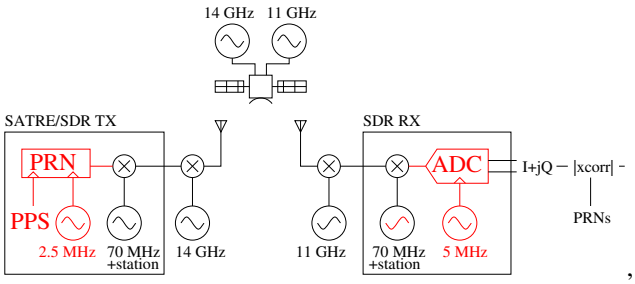

Figure 28. Communication chain between ground-satellite-ground with the varying local oscillators along the link

uplink is under control but the satellite shifts from 14 GHz to 11 GHz the incident signal to the downlink frequency, which is finally received on the ground by a microwave oscillator which might or might not be controlled by a metrological reference. Hence, only the code provided by the periodic correlation peaks is usable, since the intermediate frequency shifts are not controlled (Fig. 28).

This adventure has most significantly been the opportunity to address new radiofrequency signals by receiving and decoding information broadcast by a geostationary satellite, for a minimal cost considering the availability of left over television satellite receiving parabola antennas and the ability to feed a 20 euro software defined radio with such signals.

The repository summarizing these developments is available at `https://github.com/oscimp/gr-satre` and is looking for external contributors to add the missing elements of a fully functional decoding system.

Acknowledgements

This investigation is a side effect of a project funded by Laboratoire d'Excellence (Labex) FIRST-TF between SYRTE/Paris Observatory, OSU Theta/Besançon Observatory and the Time and Frequency department of the FEMTO-ST Institute. The information shared in this document are all publicly available for those looking long enough, but I (JMF) would never been able to collect in a single year all these data without having communicated with the project partners which are J. Achkar, M. Lours and M. Dupont at SYRTE as well as F. Meyer and É. Meyer at Besançon Observatory. The participant to the mailing list `time-nuts@lists.febo.com` have provided precious information, especially A. Bauch from the German PTB and F. Meynadier from BIPM are warmly acknowledged. The signals transmitted daily by national Observatories are accessible to all tax payers funding these information and even if not using practically for time and frequency dissemination, it seems at least reasonable to inform on

the nature and availability of these signals as promoted by FSFE at https://fsfe.org/activities/publiccode/publiccode.fr.html.

References

[1] C. Audoin & B. Guinot, *The measurement of time – time, frequency and the atomic clock*, Cambridge University Press (2001), Fig. 5.6 p. 105.

[2] J.-M Friedt, W. Feng, *Analyse et réalisation d'un RADAR à bruit par radio logicielle (1/3)*, *Analyse et réalisation d'un RADAR à synthèse d'ouverture (SAR) par radio logicielle (2/3)* and *Mesure fine de déplacement par RADAR interférométrique à synthèse d'ouverture (InSAR) par radio logicielle (3/3)*, GNU/Linux Magazine France 240,242 et 244 (2021)

[3] *Recommendation ITU-R TF.1153-4 – The operational use of two-way satellite time and frequency transfer employing pseudorandom noise codes* (08/2015)

[4] I. Lucresi *& al.*, *SDR-based System for Satellite Ranging Measurements*, IEEE A&E Systems Magazine 8–13 (2016) uses an X310 software defined radio and compares with SATRE

[5] Z. Jiang *& al.*, *Implementation of SDR TWSTFT in UTC Computation*, Proc. 49th Annual Precise Time and Time Interval Systems and Applications Meeting, pp. 184-208 (2018)

[6] Z. Jiang *& al.*, *Use of software-defined radio receivers in two-way satellite time and frequency transfers for UTC computation*, Metrologia **55** 685-–698 (2018)

[7] A.C. Clarke, *Extra-terrestrial relays – Can Rocket Stations Give World-wide Radio Coverage?* Wirelese World (1945), 305–

[8] CCTF/17-20, *RISE Research Institutes of Sweden, Report on Activities to the 21th meeting of the Consultative Committee for Time and Frequency, June 2017* section 7.2. Passive Utilization of TWSTFT

[9] C. Rieck, P. Jarlemark & K. Jaldehag, *Utilizing TWSTFT in a Passive Configuration*, Proc. 48th Annual Precise Time and Time Interval Systems and Applications Meeting (2017)

[10] Derek OK9SGC, *Receiving Starlink satellite beacons on a budget* (25 November 2021) at https://sgcderek.github.io/blog/starlink-beacons.html claims signals at 11325, 11575, 11950 and 12450 MHz

[11] J.-M Friedt, *Le récepteur de radio logicielle RSP1 : 8 MHz de bande passante pour moins de 20 euros* Hackable **44** (2022)

[12] Eutelsat, *Antenna and VSAT – Type Approval/Characterization – ESOG 120 – Issue 8 - Rev. 1*, May 2021 at https://www.eutelsat.com/files/contributed/satellites/pdf/esog120.pdf

[13] A. Kanj, *Étude et développement de la méthode TWSTFT phase pour des comparaisons hautes performances d'étalons primaires de fréquence*, Univ. Pierre & Marie Curie PhD Thesis (2012) with the sub-carriers described p.53

[14] V. Zhang *& al.*, *A Study on Using SDR Receivers for the Europe-Europe and Transatlantic TWSTFT Links*, Proc. 2017 Precise Time and Time Interval Meeting (2017)

[15] M.L. Psiaki *& al. Searching for Galileo: Reception and Analysis of Signals from GIOVE-A*, GPS World **17** (6) 66-72 (2006) seems unavailable but is described at https://news.cornell.edu/stories/2006/07/cornell-sleuths-crack-secret-codes-europes-galil and its links.

[16] P. Hartl, *Present state of long distance time transfer via satellites with application of the Mitrex modem* IEEE Military Communications Conference MILCOM **2** (1986)

[17] K. Imamura & F. Takahashi, *Frequency and Time Comparison – Two-way time transfer via a geostationary satellite*, J. of the Communication Research Laboratory **39**(1), 91–100 (1992)

[18] G. De Jong. *Two-way satellite time transfer: Overview and recent developments* Proc 25th Annual Precise Time and Time Interval (PTTI) (1993) at https://apps.dtic.mil/sti/pdfs/ADA280955.pdf#page=112

[19] Y. Guidon, *Comprendre les générateurs de nombres pseudo-aléatoires*, GNU/Linux Magazine France **81** 64–76 (2006) et *Sciences/Théorie de l'information : propriétés et dérivés des CRC et LFSR*, GNU/Linux Magazine France **85** 84–93 (2006)

[20] J.-M Friedt, C. Droit, G. Martin, and S. Ballandras, *A wireless interrogation system exploiting narrowband acoustic resonator for remote physical quantity measurement*, Rev. Sci. Instrum. **81** 014701 (2010)

[21] J.-M Friedt, G. Cabodevila, *Exploitation de signaux des satellites GPS reçus par récepteur de télévision numérique terrestre DVB-T*, OpenSilicium **15** (2015)

[22] M. Marazin, R. Gautier, G. Burel, *Dual Code Method for Blind Identification of Convolutional Encoder for Cognitive Radio Receiver Design*, Proc IEEE GLOBECOM Workshops (2009)

[23] C. Rieck, P. Jarlemark & K. Jaldehag, *Passive Utilization of the TWSTFT Technique*, Proc EFTF (2018)

[24] J.-M Friedt, C. Eustache, É. Carry, E. Rubiola, *Software defined radio decoding of DCF77: time and frequency dissemination with a sound card*, Radio Science **53** (1) 48–61 (2018)

[25] https://rhodesmill.org/skyfield/installation.html

[26] T.S. Kelso, *Validation of SGP4 and IS-GPS-200D Against GPS Precision Ephemerides*, Proc. 17th AAS/AIAA Space Flight Mechanics Conference (2017), AAS 07-127 at https://celestrak.com/publications/AAS/07-127/AAS-07-127.pdf whose figure 2 illustrates the divergence of predicting medium-Earth orbiting GPS satellite position with respect to observations

[27] D.A. Vallado, P. Crawford, R. Hujsak, T.S. Kelso, *Revisiting Spacetrack Report #3: Rev 3*, Proc. AIAA/AAS Astrodynamics Specialist Conference (2006) at https://celestrak.org/publications/AIAA/2006-6753/AIAA-2006-6753-Rev3.pdf